Generalized Classical Axially Symmetric Dual-Reflector Antennas

Fernando J. S. Moreira, *Member, IEEE,* and Aluizio Prata, Jr., *Member, IEEE*

***Abstract*—This work presents a generalized study of classical axially symmetric dual-reflector antennas. The antenna dishes are simply described by conic sections, arranged to reduce the main-reflector radiation toward the subreflector surface. The dual-reflector configuration provides a uniform-phase field distribution over the illuminated portion of the aperture, starting from a spherical-wave feed source at the antenna primary focus. All possible configurations are characterized into a total of four distinct groups. Simple closed-form design equations and the aperture field distribution are derived, in a unified way, for all these kinds of generalized antennas using the principles of geometrical optics. The formulation is applied in a parametric study to establish the configurations yielding maximum radiation efficiency (not including diffraction effects). The design procedure is exemplified in the synthesis of a novel configuration, which is further analyzed by the moment method.**

***Index Terms*—Aperture fields, design methodology, electromagnetic reflection, geometrical optics, reflector antennas.**

I. Introduction

CLASSICAL axially symmetric Cassegrain and Gregorian reflectors have been used for many years in high-gain antenna applications [1], [2]. The main disadvantage of these configurations is the subreflector blockage, which causes a number of deleterious effects such as the decrease of the antenna aperture efficiency. However, this problem can be minimized by reducing the main-reflector radiation toward the subreflector. This may be accomplished by either shaping both reflectors [3] or using alternative classical configurations, where the generating curves of the axially symmetric reflectors are described by conic sections [4]–[8]. In this paper, the second option is considered by presenting generalized classical axially symmetric dual-reflector antennas that prevent, from a geometrical optics (GO) standpoint, the main-reflector scattered energy from striking the subreflector surface while providing a uniform-phase aperture distribution. A closed-form design procedure (starting from relevant geometrical parameters) and the GO aperture field are established, in a unified way, for all possible configurations. The formulation to be presented can be applied to determine the optimum classical geometry.

The next section introduces the basic parameters of the generalized classical axially symmetric dual-reflector antennas. It is shown that all possible configurations can be characterized into four distinct groups, according to the location of the subreflector caustics. Starting from five relevant geometrical parameters, the antenna closed-form design equations are derived in Section III. The design procedure is of easy implementation and use, as it is general and no transcendental equations are required. The GO aperture-field distribution is obtained in Section IV. Although the GO principles do not account for diffraction mechanisms, the results are very useful for design purposes. From the GO aperture fields, a parametric study is conducted in Section V in order to determine the antenna geometries providing maximum radiation efficiency. In Section VI, a case study is conducted to demonstrate the design procedure, where the moment method is applied to analyze the resulting antenna. This paper is concluded in Section VII.

Manuscript received November 20, 1998; revised September 11, 2000. The work of F. J. S. Moreira was supported in part by the Brazilian agency CNPq.

F. J. S. Moreira is with the Department of Electronics Engineering, Federal University of Minas Gerais, Belo Horizonte, MG 30161-970 Brazil.

A. Prata, Jr., is with the Department of Electrical Engineering-Electrophysics, University of Southern California, Los Angeles, CA 90089-0271 USA.

Publisher Item Identifier S 0018-926X(01)01843-9.

II. Generalized Classical Axially Symmetric Dual-Reflector Geometries

There are four distinct types of classical axially symmetric dual-reflector antennas that avoid the main-reflector scattering toward the subreflector. Their generating curves and relevant parameters are depicted in Figs. 1–4. They are obtained from GO concepts by imposing a uniform-phase field distribution over the antenna aperture, starting from a spherical-wave feed source at the antenna primary focus (point O, the origin). The three-dimensional reflector surfaces are yielded by spinning the generating curves about the z-axis (symmetry axis). At the $y = 0$ plane of Figs. 1–4, the basic geometrical parameters of the four configurations are defined as follows. D_M and D_S are the main and subreflector diameters, respectively. D_B is the blockage diameter, and the condition $D_S \leq D_B < D_M$ provides the subreflector clearance. V_M and V_S are the z-coordinates of the main and subreflector points corresponding to the feed principal ray, respectively. F is the focal length of the parabola generating the main reflector, and $2c$ and e are the interfocal distance and eccentricity of the hyperbola or ellipse generating the subreflector, respectively. θ_E is the subreflector edge angle and β is the tilt angle between the z-axis and the axis of the subreflector generating conic section. θ_L and θ_U are the lower and upper angles of the main reflector, respectively. Finally, the angle θ_F defines an arbitrary feed-ray direction in the $y = 0$ plane (such that $|\theta_F| \leq |\theta_E|$), with a corresponding main-reflector angle θ_M. It is important to note that in this paper, positive (negative) angular values correspond to counterclockwise (clockwise) angles in the $y = 0$ plane shown in Figs. 1–4.

The four classical configurations are basically characterized by the location of the two subreflector caustic regions. One caustic (a ring caustic) is located by the rotation of the parabola focal point (point P) about the symmetry axis. The second

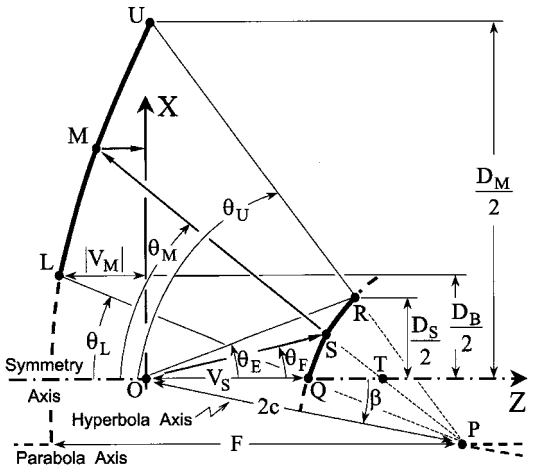

Fig. 1. Basic geometry of the axially displaced Cassegrain configuration.

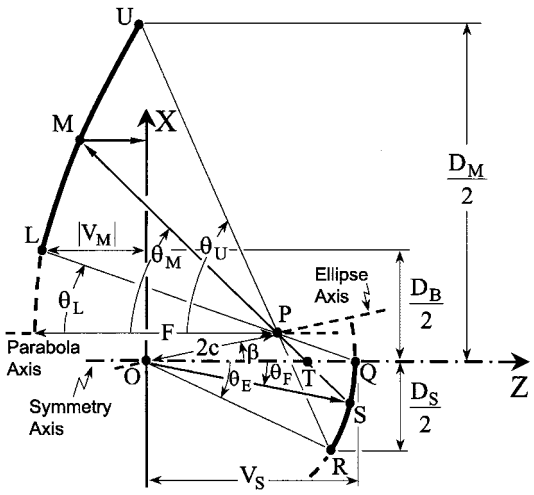

Fig. 2. Basic geometry of the axially displaced Gregorian configuration.

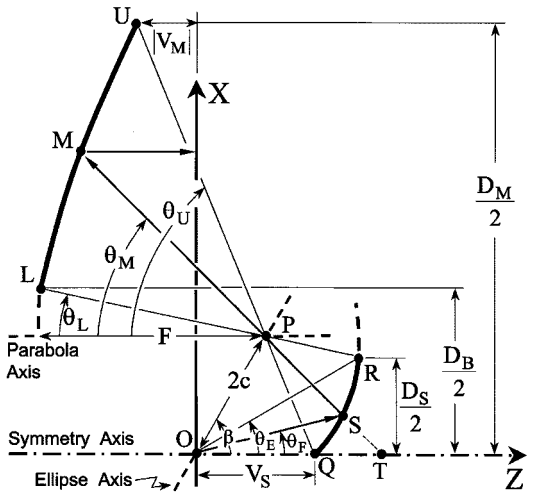

Fig. 3. Basic geometry of the axially displaced ellipse configuration.

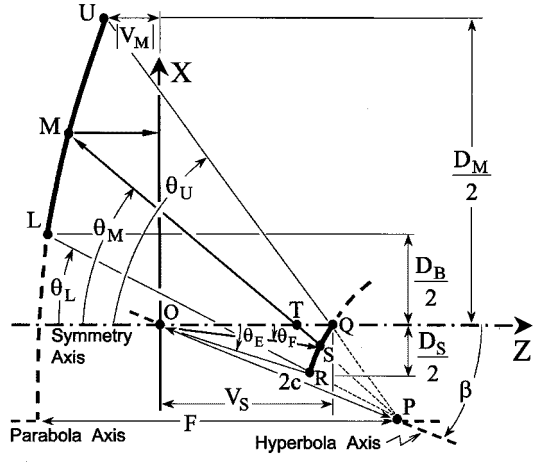

Fig. 4. Basic geometry of the axially displaced hyperbola configuration.

caustic (a line caustic) corresponds to the portion of the symmetry axis intersected by the subreflector reflected rays (point T). The first geometry (Fig. 1) has virtual ring and line caustics and is classified here as an axially displaced Cassegrain (ADC). This geometry was previously studied in [5] and named axially tilted hyperbola (ATH). The second geometry (Fig. 2) has real ring and line caustics and is defined as an axially displaced Gregorian (ADG). The third geometry (Fig. 3) has a real ring caustic and a virtual line caustic and is named axially displaced ellipse (ADE) [6], [7]. It was previously studied in [5] under the denomination axially tilted ellipse (ATE) and is also known as the Yerukhimovichian configuration. Finally, the last configuration (Fig. 4) has a virtual ring caustic and a real line caustic and is denominated axially displaced hyperbola (ADH). In all these configurations, the main reflector is generated by a parabola, while the subreflector generating curve is either a hyperbola (ADC and ADH) or an ellipse (ADG and ADE). The feed is located at one of the hyperbola/ellipse foci (point O) and the parabola focus coincides with the other hyperbola/ellipse focus (point P). For the ADC and ADH, the hyperbola can be convex ($e > 1$) or concave ($e < -1$), and $|e| \to \infty$ yields a straight line. The basic parameters of the four antenna configurations are summarized in Table I, where the parameter X_S is the x-coordinate of the subreflector generating-curve extreme ($D_S = 2|X_S|$).

The classical Cassegrain and Gregorian configurations [1] are particular cases of the ADC and ADG, respectively, yielded by taking the limit $D_B \to 0$. The statement made in [5] about the classical Gregorian geometry's being a particular case of the ADE (or ATE) is incorrect.

III. Closed-Form Design Equations

From the previous discussion and Figs. 1–4, the geometry of a given generalized classical configuration is uniquely determined once the following parameters are established: the conic-section parameters F, e, and $2c$, the tilt angle β, and the edge angle θ_E (which ultimately defines the antenna aperture region). So, five input parameters are needed and, for design purposes, a suitable set is composed by $D_M, D_S = 2|X_S|, D_B, \theta_E$, and ℓ_o, where ℓ_o is the total path length from the feed to the antenna aperture (assumed at the plane $z = 0$). Note from Figs. 1–4 that $\ell_o/2$ is approximately equal to the distance between the main

TABLE I
PARAMETERS OF THE GENERALIZED CLASSICAL GEOMETRIES

ADC	ADG	ADE	ADH
$\lvert e\rvert > 1$	$0 < e < 1$	$0 < e < 1$	$\lvert e\rvert > 1$
$-\pi < \beta \leq 0$	$0 \leq \beta < \pi$	$0 < \beta < \pi$	$-\pi < \beta < 0$
$0 < \theta_E < \pi$	$-\pi < \theta_E < 0$	$0 < \theta_E < \pi$	$-\pi < \theta_E < 0$
$0 \leq \theta_F \leq \theta_E$	$\theta_E \leq \theta_F \leq 0$	$0 \leq \theta_F \leq \theta_E$	$\theta_E \leq \theta_F \leq 0$
$\theta_M < 0$	$\theta_M < 0$	$\theta_M < 0$	$\theta_M < 0$
$X_S = D_S/2$	$X_S = -D_S/2$	$X_S = D_S/2$	$X_S = -D_S/2$
$D_1 = D_B$	$D_1 = D_B$	$D_1 = D_M$	$D_1 = D_M$
$D_2 = D_M$	$D_2 = D_M$	$D_2 = D_B$	$D_2 = D_B$
$\theta_1 = \theta_L < 0$	$\theta_1 = \theta_L < 0$	$\theta_1 = \theta_U < 0$	$\theta_1 = \theta_U < 0$
$\theta_2 = \theta_U < 0$	$\theta_2 = \theta_U < 0$	$\theta_2 = \theta_L < 0$	$\theta_2 = \theta_L < 0$

and subreflector surfaces (the antenna length). All expressions to be derived in this section are valid for the four different configurations as far as the sign convention previously adopted is observed (see Table I).

To obtain the generating-curve parameters, the equations describing the conic sections are defined as follows. The parabola generating the main reflector in Figs. 1–4 is described by

$$\overline{PM} = \frac{2F}{1+\cos\theta_M} \tag{1}$$

where $\overline{PM}$ is the distance from the parabola focal point P to the main-reflector point M. The conic section generating the subreflector is described by

$$\overline{OS} \pm \overline{SP} = \frac{2c}{e} \tag{2}$$

where $\overline{OS}$ is the distance from point O to the subreflector point S, $\overline{SP}$ is the distance from point S to P, and the positive (negative) sign corresponds to the ellipse (hyperbola) conic section.

Starting from the five input parameters, the design process first establishes the values of θ_1 and θ_2 (see Table I), then the values of β and V_S, and finally the conic-section parameters $2c, e$, and F. From Figs. 1–4 one directly obtains

$$\tan\theta_1 = \frac{-D_1}{2(V_S - V_M)} \tag{3}$$

where, accordingly to Table I, the negative angle θ_1 is either θ_L or θ_U and D_1 is either D_B or D_M, depending on the adopted configuration. From the same figures, the constant path lengths associated with the principal-ray ($\theta_F = 0$) and the subreflector-edge-ray ($\theta_F = \theta_E$) directions are given by

$$\ell_o = (V_S - V_M)\left(1 + \frac{1}{\cos\theta_1}\right) \tag{4}$$

$$\ell_o = \frac{X_S}{\sin\theta_E} - \frac{X_S}{\tan\theta_E} - \frac{D_2/2 - X_S}{\sin\theta_2} - \frac{D_2/2 - X_S}{\tan\theta_2} \tag{5}$$

respectively, where the negative angle θ_2 is either θ_U or θ_L and D_2 is either D_M or D_B (see Table I). Combining (3) and (4), θ_1 is obtained from

$$\tan\left(\frac{\theta_1}{2}\right) = \frac{-D_1}{2\ell_o} \tag{6}$$

and, from (5), θ_2 is then calculated as

$$\tan\left(\frac{\theta_2}{2}\right) = \frac{-D_2 + 2X_S}{2\ell_o - 2X_S\tan(\theta_E/2)}. \tag{7}$$

To derive the remaining antenna parameters, one applies (2) and the law of sines to the triangle OPQ in Figs. 1–4 to obtain

$$\frac{-2c}{\sin\theta_1} = \frac{V_S}{\sin(\beta - \theta_1)} = \frac{2c/e - V_S}{\sin\beta} \tag{8}$$

and also to the triangle OPR to obtain

$$\frac{2c}{\sin(\theta_E - \theta_2)} = \frac{X_S/\sin\theta_E}{\sin(\beta - \theta_2)} = \frac{2c/e - X_S/\sin\theta_E}{\sin(\beta - \theta_E)}. \tag{9}$$

The combination of (8) and (9) yields

$$\frac{\sin\theta_1}{\sin\beta + \sin(\beta - \theta_1)} = \frac{-\sin(\theta_E - \theta_2)}{\sin(\beta - \theta_2) + \sin(\beta - \theta_E)} \tag{10}$$

which can be trigonometrically manipulated to establish β

$$\tan\beta = \frac{\sin\theta_E + \sin\theta_2 + \sin(\theta_E - \theta_2)}{\cos\theta_E + \cos\theta_2 + \sin(\theta_E - \theta_2)/\tan(\theta_1/2)} \tag{11}$$

where the quadrant ambiguity of β is removed using Table I. From (8) and (9), V_S is then given by

$$V_S = \frac{-X_S\sin(\theta_E - \theta_2)\sin(\beta - \theta_1)}{\sin\theta_E\sin\theta_1\sin(\beta - \theta_2)}. \tag{12}$$

The parameter V_S is an important result in the design process, as it indicates if the feed phase center is prohibitively close to the subreflector vertex or, on the other extreme, behind the main reflector. Although V_M is not directly needed to obtain the desired antenna parameters, it is a useful information and sometimes necessary to establish the initial condition of the differential equation to be solved in a GO shaping process [3]. At this point, V_M can be calculated from (3). Note that although V_S is always a positive quantity, V_M may assume either positive or negative values (see Figs. 1–4).

With the values of $\theta_1, \theta_2, \beta$, and V_S established from (6), (7), (11), and (12), respectively, the conic-section parameters are finally obtained. From (8) and (9), the interfocal distance $2c$ and the eccentricity e of the conic section generating the subreflector are given by

$$2c = \frac{-V_S\sin\theta_1}{\sin(\beta - \theta_1)} \tag{13}$$

$$e = \frac{-\sin\theta_1}{\sin\beta + \sin(\beta - \theta_1)}. \tag{14}$$

From Figs. 1–4 and (1) (with $\theta_M = \theta_1$), the parabola focal length F is then calculated

$$F = \frac{-D_1 + 4c\sin\beta}{4\tan(\theta_1/2)}. \tag{15}$$

The commonly encountered classical Cassegrain and Gregorian configurations [1] can be directly obtained from the ADC and ADG, respectively, by taking the limit $D_B \to 0$ in (3)–(15) [8].

An important issue concerning the antenna designer regards the blockage effects. For the present antenna geometries, three blockage mechanisms may be present (according to GO concepts and not considering the blockage provided by the subreflector supporting structure): subreflector, feed, and self blockages. The subreflector blockage is characterized by the incidence of main-reflector reflected rays upon the subreflector. It is avoided when $D_S \leq D_B < D_M$ (see Figs. 1–4). The feed blockage occurs when part of the subreflector reflected rays impinges upon the feed structure, depending on the feed physical dimensions. The adopted formulation assumes a feed illumination provided by a point source. Under this condition, the feed blockage never occurs for the ADC and ADE (see Figs. 1 and 3, respectively). For the ADG and ADH, it is avoided providing that the subreflector real line caustic is located between the primary focus (point O) and the subreflector vertex (point Q). From Figs. 2 and 4, this is accomplished whenever

$$|\theta_E| \leq |\theta_2|. \tag{16}$$

The self blockage refers to the intersection of rays reflected by the subreflector lower (upper) half with the subreflector upper (lower) half surface, which can only occur for the ADG and ADH configurations (see Figs. 1–4). The geometric conditions for the avoidance of such blockage mechanism are found in [8].

IV. GO Aperture Field Distribution

The basic antenna radiation characteristics (e.g., gain, efficiency, radiation pattern, etc.) can be calculated from the GO aperture field distribution. However, diffraction effects are ignored by GO, and this might be a significant source of inaccuracy in all but reflector systems with very large electric dimensions (where GO is the dominant effect). Besides the diffraction effects, the GO aperture field distribution also neglects the direct feed contribution to the antenna radiation pattern, multiple bounces over the reflector structure, etc. In any event, for antenna design purposes, the information contained in the GO aperture distribution is very useful.

The GO field distribution over the aperture plane is obtained from the geometries in Figs. 1–4 and from the corresponding conic-section equations [(1) and (2)]. On doing so, one must recall that Figs. 1–4 represent the reflector generating curves in the $y = 0$ plane—the three-dimensional configurations are obtained by spinning these curves about the symmetry axis. The feed spherical-wave radiation is assumed equal to

$$\vec{E}_F(\vec{r}_F) = [E_\theta(\theta_F, \phi_F)\hat{\theta}_F + E_\phi(\theta_F, \phi_F)\hat{\phi}_F] \times \frac{\exp(-jk_o r_F)}{r_F} \tag{17}$$

where $\vec{E}_F(\vec{r}_F)$ is the electric field of the feed TEM radiation; $k_o = 2\pi/\lambda_o$; and r_F, θ_F, and ϕ_F are the spherical coordinates associated with the feed system (such that $|\theta_F| \leq |\theta_E|$, according with the previously adopted angular notation). Equation (17) allows the representation of most practical feeds, assumed sufficiently away from the subreflector.

The aperture cylindrical coordinates ρ_A and ϕ_A are defined as usual. Using GO concepts and Figs. 1–4, one observes that, after the reflection by the two surfaces, the feed electric field polarized in the positive (negative) $\hat{\theta}_F$-direction is mapped at the aperture in the positive $\hat{\rho}_A$-direction, and the feed electric field polarized in the positive (negative) $\hat{\phi}_F$-direction is mapped at the aperture in the positive $\hat{\phi}_A$-direction for the ADC and ADE (ADG and ADH) configurations. As the aperture field has a uniform phase distribution, the GO electric-field Cartesian components E_X^A and E_Y^A at the aperture plane are then given by

$$\begin{bmatrix} E_X^A(\rho_A, \phi_A) \\ E_Y^A(\rho_A, \phi_A) \end{bmatrix} = \begin{bmatrix} \cos\phi_A & -\sin\phi_A \\ \sin\phi_A & \cos\phi_A \end{bmatrix} \begin{bmatrix} E_\theta(\theta_F, \phi_F) \\ E_\phi(\theta_F, \phi_F) \end{bmatrix} \times \cos(\phi_F - \phi_A)\,\mathcal{A}(\theta_F)\exp[j(\Phi_G - k_o\ell_o)] \tag{18}$$

where Φ_G is the Gouy phase shift [9] and $\mathcal{A}(\theta_F)$ is the amplitude of the GO aperture fields. The relation between ϕ_F and ϕ_A is obtained from

$$|\phi_F - \phi_A| = \begin{cases} 0, & \text{for the ADC and ADE} \\ \pi, & \text{for the ADG and ADH.} \end{cases} \tag{19}$$

The Gouy phase shift Φ_G is obtained by adding a $\pi/2$ phase shift each time the ray trajectory crosses a real caustic [9]. From Figs. 1–4, one then has

$$\Phi_G = \begin{cases} 0, & \text{for the ADC} \\ \pi/2, & \text{for the ADE and ADH} \\ \pi, & \text{for the ADG.} \end{cases} \tag{20}$$

The amplitude $\mathcal{A}(\theta_F)$ is obtained using GO concepts, with the help of (1), (2), and Figs. 1–4. The expressions to be derived are valid for all the generalized classical antennas, as long as one observes the previously defined sign convention (see Table I). $\mathcal{A}(\theta_F)$ is represented as [10]

$$\mathcal{A}(\theta_F) = \frac{1}{r_F}\sqrt{\left|\frac{\rho_{1r}^S \rho_{2r}^S}{\left(R_{\mathrm{SM}} + \rho_{1r}^S\right)\left(R_{\mathrm{SM}} + \rho_{2r}^S\right)}\right|} \tag{21}$$

where

- r_F distance between the primary focus and the subreflector surface along the feed ray θ_F (segment $\overline{OS}$);
- R_{SM} distance between the sub- and main-reflector surfaces along the reflected ray (segment $\overline{SM}$);
- ρ_{1r}^S and ρ_{2r}^S subreflector-reflected wavefront principal radii of curvature at point S (associated with the ring and line caustics, respectively).

ρ_{1r}^S and ρ_{2r}^S are positive (divergent wave) or negative (convergent wave) if the corresponding caustics are virtual or real, respectively. The absolute values of ρ_{1r}^S and ρ_{2r}^S are given by the lengths of $\overline{SP}$ and $\overline{ST}$, respectively. From Figs. 1–4 and (2), the distance r_F is given by

$$r_F = \frac{c(e - 1/e)}{e\cos(\beta - \theta_F) - 1} \tag{22}$$

and the principal radius of curvature ρ_{1r}^S is given by

$$\rho_{1r}^S = r_F - \frac{2c}{e}. \tag{23}$$

Note that (23) already takes into account the correct sign of ρ_{1r}^S for the different classical geometries. The distance $R_{\rm SM}+\rho_{1r}^S$ corresponds to the length of $\overline{PM}$, which is given by (1) as

$$R_{\rm SM}+\rho_{1r}^S=\frac{2F}{1+\cos\theta_M}. \tag{24}$$

Applying the law of sines to the triangle OTS in Figs. 1–4, the principal radius of curvature ρ_{2r}^S is given by

$$\rho_{2r}^S=\frac{-r_F\sin\theta_F}{\sin\theta_M} \tag{25}$$

noticing that θ_M is a negative angle. Similarly to ρ_{1r}^S in (23), this equation already accounts for the sign of ρ_{2r}^S. The distance $R_{\rm SM}+\rho_{2r}^S$ corresponds to the length of $\overline{TM}$ and is obtained from (1) and by applying the law of sines to the triangle OPT

$$R_{\rm SM}+\rho_{2r}^S=\frac{2F}{1+\cos\theta_M}-\frac{2c\sin\beta}{\sin\theta_M}. \tag{26}$$

In order to eliminate θ_M from (24)–(26), one uses the following relation, obtained from Figs. 1–4 and (2)

$$\tan\left(\frac{\beta-\theta_F}{2}\right)=\left(\frac{1-e}{1+e}\right)\tan\left(\frac{\beta-\theta_M}{2}\right). \tag{27}$$

Finally, the substitution of (22)–(27) into (21) yields, after straightforward algebraic manipulations, the desired expression for $\mathcal{A}(\theta_F)$ of (18)

$$\mathcal{A}(\theta_F)=\sqrt{\left|\frac{\tan(\theta_F/2)[A_1(\theta_F)-A_2(\theta_F)]^3}{4F(e^2-1)[A_3(\theta_F)-A_4(\theta_F)]}\right|} \tag{28}$$

where

$$A_1(\theta_F)=(1-e\cos\beta)(1+\cos\theta_F) \tag{29}$$
$$A_2(\theta_F)=e\sin\beta\sin\theta_F \tag{30}$$
$$A_3(\theta_F)=[c(1-e\cos\beta)+eF]\sin\beta(1+\cos\theta_F) \tag{31}$$
$$A_4(\theta_F)=[F(1+e\cos\beta)+ce\sin^2\beta]\sin\theta_F. \tag{32}$$

The relation between θ_F and ρ_A, obtained from (1) and (27), is given by

$$\tan\left(\frac{\theta_F}{2}\right)=\frac{e(\sin\beta+\Delta\cos\beta)-\Delta}{e(\cos\beta-\Delta\sin\beta)+1} \tag{33}$$

where

$$\Delta=-\tan\left(\frac{\theta_M}{2}\right)=\frac{\rho_A-2c\sin\beta}{2F}. \tag{34}$$

Note that the correct sign of θ_F is already taken into account by (33).

V. Configurations for Maximum Efficiency

In this section, a parametric study is conducted to determine the geometries providing maximum radiation efficiency, based on the GO aperture distribution derived in the previous section. The feed is modeled as an $\hat{x}$-polarized circularly symmetric raised-cosine feed (RCF) [11], in which case (18) reduces to [8]

$$\vec{E}^A(\rho_A)=\cos^h\theta_F\mathcal{A}(\theta_F)\exp[j(\Phi_G-k_o\ell_o)]\hat{x} \tag{35}$$

where the parameter h controls the circularly symmetric pattern of the RCF model. Instead of characterizing the RCF from h, it is preferable to define its far-zone taper F_t toward $\theta_F=\theta_E$, given by

$$F_t=20h\log_{10}(\cos\theta_E). \tag{36}$$

The antenna radiation efficiency η is calculated from

$$\eta=G_o(\pi D_M/\lambda_o)^{-2} \tag{37}$$

where G_o is the antenna boresight gain calculated from the far-zone radiation of the GO aperture distribution given by (35) and accounting for the total feed power [11]. Due to the GO concepts used to derive (35), the efficiency η is identical for similar antennas when the same feed illumination is applied [11]. An antenna is considered similar to another if they only differ by a scale factor. Under a GO perspective, it is then possible to study the efficiencies of different geometries using any one of the antenna linear dimensions as a normalization factor (in this work, D_M is this factor). So, the efficiency of a desired generalized classical configuration is obtained once the values of $D_S/D_M, D_B/D_M, \ell_o/D_M, \theta_E$, and F_t are specified.

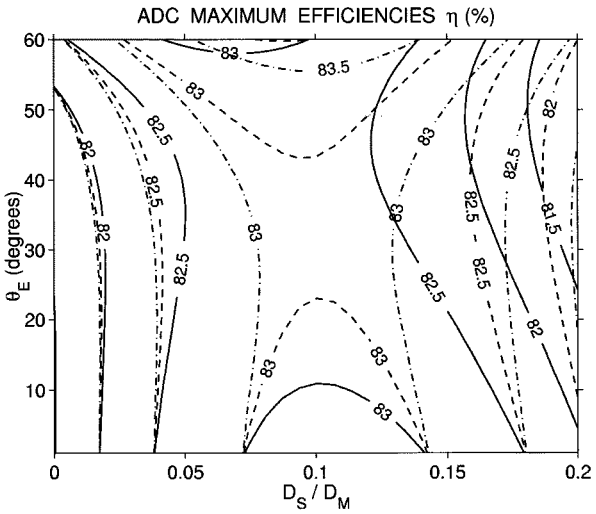

(a)

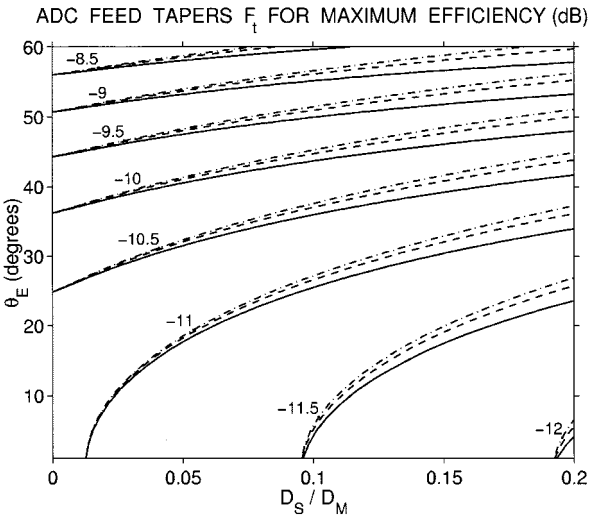

(b)

Fig. 5. ADC (a) maximum efficiencies η and (b) corresponding feed tapers. F_t: $\ell_o/D_M=0.5$ (solid lines), 1 (dashed lines), and 2 (dash-dot lines).

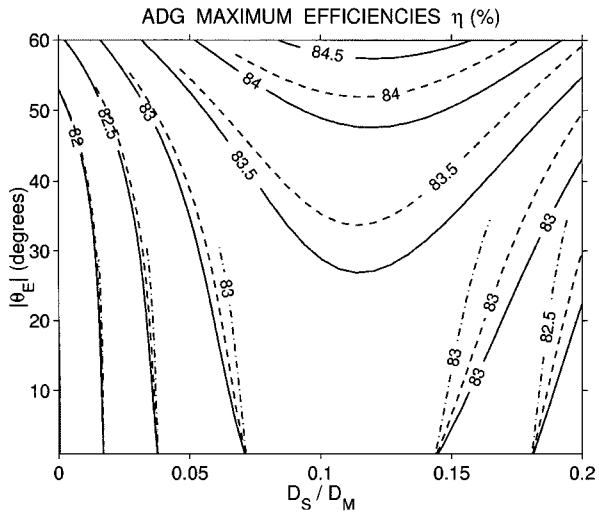

(a)

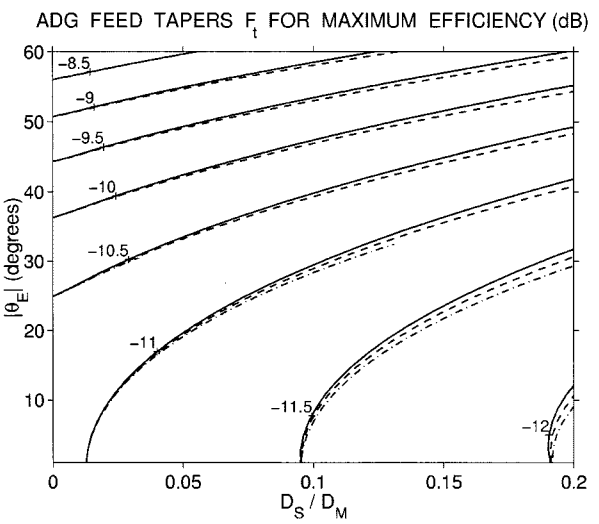

(b)

Fig. 6. ADG (a) maximum efficiencies η and (b) corresponding feed tapers F_t: $\ell_o/D_M = 0.7$ (solid lines), 1 (dashed lines), and 2 (dash-dot lines).

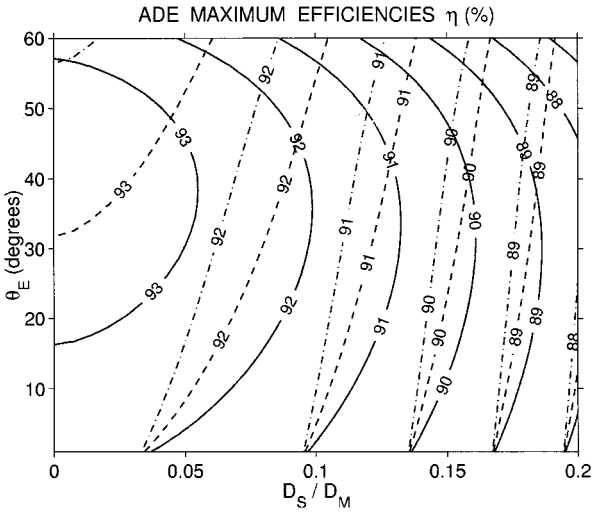

(a)

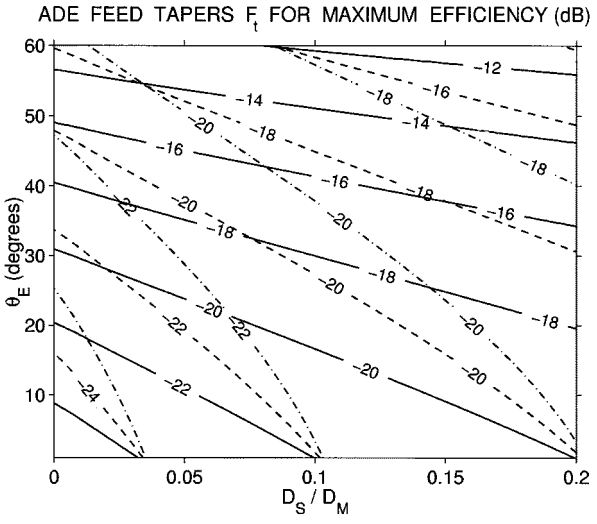

(b)

Fig. 7. ADE (a) maximum efficiencies η and (b) corresponding feed tapers F_t: $\ell_o/D_M = 0.5$ (solid lines), 1 (dashed lines), and 2 (dash-dot lines).

In order to provide the maximum illuminated aperture area, D_B is always assumed equal to D_S. The parametric study is performed by varying the values of D_S/D_M $(0 < D_S/D_M \leq 0.2)$, θ_E $(0° < |\theta_E| \leq 60°)$, and ℓ_o/D_M $(0.5 \leq \ell_o/D_M \leq 2)$. For each triplet, the values of η and F_t (yielding the maximum η) are then obtained. The resulting η values and the corresponding F_t values are shown for the ADC (Fig. 5), ADG (Fig. 6), ADE (Fig. 7), and ADH (Fig. 8) configurations.

The efficiencies of the ADC and ADG approximately have the same behavior (Figs. 5 and 6, respectively). Their maximum values are about 83%, occuring when $D_S/D_M \approx 0.1$ and $F_t \approx -11$ dB. These results come as no surprise as, for small D_S/D_M values, the geometries approximate the classical Cassegrain and Gregorian configurations, respectively. So, applying the equivalent-paraboloid principle, the maximum $\eta \approx 83\%$ with $F_t \approx -11$ dB is expected [11]. As explained at the end of Section III, feed and self blockages may occur for the ADG. It was observed that in the adopted ranges of D_S/D_M and $|\theta_E|$, the self blockage is only avoided for $\ell_o/D_M \geq 0.7$. As the value of ℓ_o/D_M is increased, feed blockage becomes the concern. In Fig. 6, the contour lines are abruptly interrupted in the regions where the feed blockage is at play. From this figure, when $\ell_o/D_M = 1$, the feed blockage appears for small values of D_S/D_M and large $|\theta_E|$ values. For $\ell_o/D_M = 2$, this blockage mechanism occurs whenever $|\theta_E| > 35°$.

The ADE and ADH provide maximum efficiencies around 91% (see Figs. 7 and 8, respectively), somewhat higher than those obtained by the ADC and ADG. This is due to the converse of the feed energy redistribution in the aperture plane [5]. The results indicate that η is improved as $D_S/D_M \to 0$, which permits the use of relatively small subreflectors without compromising the antenna performance. Furthermore, these high efficiencies are obtained in conjunction with large values of $|F_t|$, which indicates that reduced forward spillover can also be attained. However, the self and feed blockages are of great concern for the ADH configuration. In the present ranges of D_S/D_M and $|\theta_E|$, the self blockage stops to occur only when $\ell_o/D_M > 0.9$ (only the results for $\ell_o/D_M = 1$ and 2 are shown

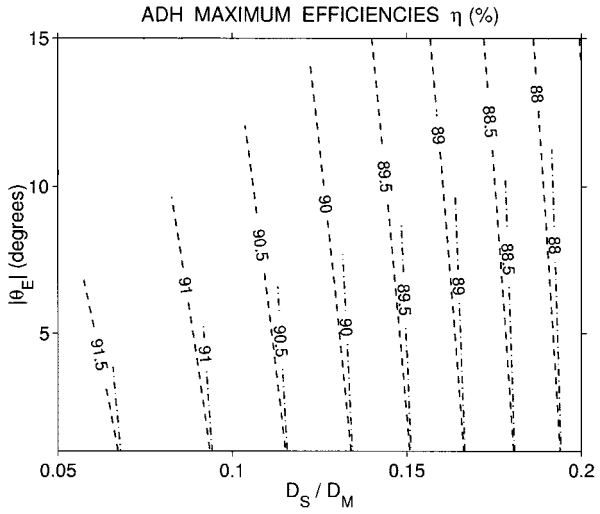

(a)

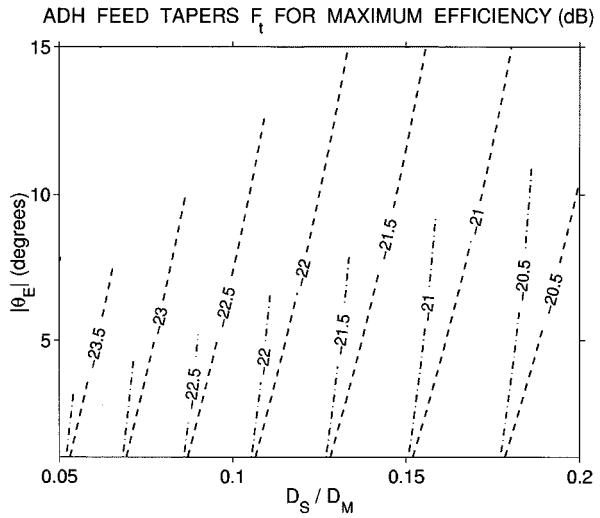

(b)

Fig. 8. ADH (a) maximum efficiencies η and (b) corresponding feed tapers F_t: $\ell_o/D_M = 1$ (dashed lines) and 2 (dash-dot lines).

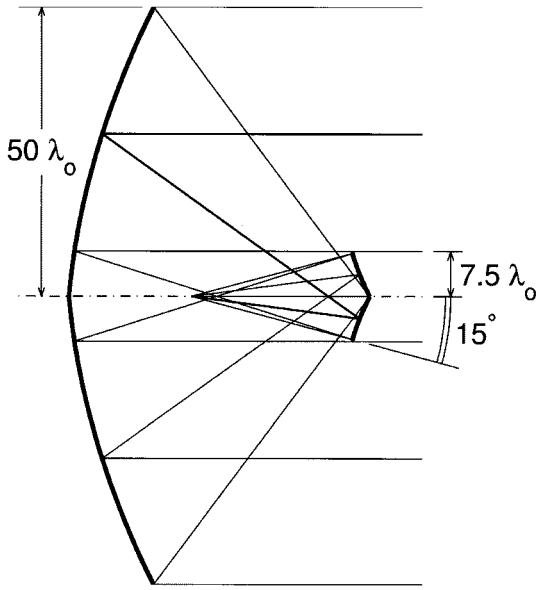

(a)

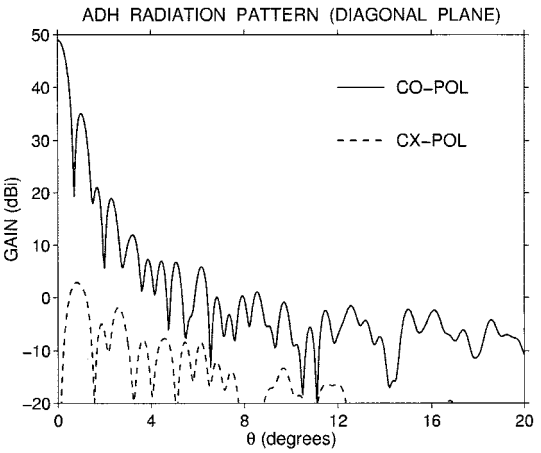

(b)

Fig. 9. ADH configuration with $D_M = 100\lambda_o, D_S = D_B = 15\lambda_o, \theta_E = -15°, \ell_o = 100\lambda_o$, and $F_t = -21.5$ dB: (a) geometry and (b) MoM radiation pattern.

in Fig. 8). The feed blockage is always present when $|\theta_E| > 20°$ and the contour lines in Fig. 8 are interrupted whenever this blockage is in action.

VI. ADH Case Study

To demonstrate the design procedure of the present antennas, the novel ADH configuration (see Fig. 4) is adopted. The resulting dual-reflector antenna is analyzed by the method of moments (MoM) [8] to establish the diffraction effects to the antenna efficiency (which are not considered in the previously presented theory). D_M is set equal to $100\lambda_o$. Although the results of Fig. 8 indicate that higher efficiencies are obtained for smaller subreflectors, $D_S = D_B = 15\lambda_o$ to minimize the effects of the subreflector diffraction. To avoid blockage mechanisms, $\ell_o = 100\lambda_o$ and $|\theta_E| = 15°$ (see Fig. 8, noting that $\theta_E < 0$ for the ADH). From Fig. 8, a maximum efficiency $\eta \approx 89\%$ is expected with $F_t \approx -21.5$ dB [$h \approx 72$ from (36)]. The antenna excitation is provided by a linearly polarized improved raised-cosine feed model (IRCF). The IRCF correctly accounts for the near- and far-zone electromagnetic behavior of the feed, departing from an initial RCF model [12]. The adopted IRCF has parameters $h = 72, a = 30\lambda_o, A = 1$, and $\Psi = 0°$, according to (36) and [12].

From the above input parameters, the values of $\theta_1 = \theta_U = -53.13°, \theta_2 = \theta_L = -17.23°, \beta = -15.64°, V_S = 30.96\lambda_o$, $V_M = -6.54\lambda_o, 2c = 40.70\lambda_o$, $e = 2.360\,159$, and $F = 60.97\lambda_o$ are obtained from (6), (7), (11), (12), (3), and (13)–(15), respectively. The resulting antenna is depicted in scale in Fig. 9(a). To avoid diffraction from the main-reflector internal rim (see Fig. 4), its surface is extended toward the symmetry axis (using its generating parabola). From Fig. 9(a), one observes that the reflected rays departing from the subreflector rim almost intersect the antenna primary focus. However, this does not arouse great concerns regarding feed

blockage, as the corresponding reflected field is highly tapered ($F_t \approx -21.5$ dB). The antenna radiation pattern (obtained from the MoM analysis, including the IRCF rediation) in the diagonal plane is shown in Fig. 9(b). The antenna gain is 48.96 dBi, corresponding to a radiation efficiency of 79.7%, which is approximately 9% smaller than the result of Fig. 8(a) due to the diffraction effects. The cross-polarization peak is 2.9 dBi at $\theta = 0.8°$, corresponding to a large polarization isolation of about 46 dB. The copolarization gain at $\theta = 15°$ is about -2 dBi, corresponding to an expectedly small feed spillover.

VII. Conclusion

This paper presented, in a generalized way, all possible classical axially symmetric dual-reflector antennas providing a uniform-phase aperture distribution from a spherical-wave point source located at the antenna primary focus. These antennas are characterized into four distinct configurations: the axially displaced Cassegrain, Gregorian, ellipse, and hyperbola. Useful closed-form design equations and aperture-field expressions were uniformly derived for all configurations from geometrical optics concepts. These expressions were then used in a parametric study to establish the conditions for maximum radiation efficiency. It was found that the ADC and ADG can provide, without considering any diffraction effects, efficiencies up to 84%, while the ADE and ADH can reach efficiencies beyond 90% with reduced feed spillovers and relatively smaller subreflector diameters. The design procedure was exemplified with the novel ADH configuration and its radiation characteristics further analyzed by the moment method for the sake of completeness.

References

[1] P. W. Hannan, "Microwave antennas derived from the Cassegrain telescope," *IRE Trans. Antennas Propagat.*, vol. AP-9, pp. 140–153, Mar. 1961.

[2] W. V. T. Rusch, "Scattering from a hyperboloidal reflector in a Cassegrainian feed system," *IEEE Trans. Antennas Propagat.*, vol. AP-11, pp. 414–421, July 1963.

[3] V. Galindo, "Design of dual-reflector antennas with arbitrary phase and amplitude distributions," *IEEE Trans. Antennas Propagat.*, vol. AP-12, pp. 403–408, July 1964.

[4] J. L. Lee, "Improvements in or relating to microwave aerials," U.K. Patent 973 583, Oct. 1964.

[5] Y. A. Yerukhimovich, "Analysis of two-mirror antennas of a general type," *Telecommun. Radio Eng.*, pt. 2, vol. 27, no. 11, pp. 97–103, 1972.

[6] Yu. A. Yerukhimovich and A. Ya. Miroshnichenko, "Development of double-reflector antennas with a displaced focal axis," *Telecommun. Radio Eng.*, pt. 2, vol. 30, no. 9, pp. 90–94, 1975.

[7] W. Rotman and J. C. Lee, "Compact dual frequency reflector antennas for EHF mobile satellite communication terminals," in *Proc. IEEE AP-S Int. Symp.*, Boston, MA, June 1984, pp. 771–774.

[8] F. J. S. Moreira, "Design and rigorous analysis of generalized axially-symmetric dual-reflector antennas," Ph.D. dissertation, Univ. of Southern California, Los Angeles, Aug. 1997.

[9] M. Born and E. Wolf, *Principles of Optics*. New York: MacMillan, 1959.

[10] R. G. Kouyoumjian and P. H. Pathak, "A uniform geometrical theory of diffraction for an edge in a perfectly conducting surface," *Proc. IEEE*, vol. 62, pp. 1448–1461, Nov. 1974.

[11] S. Silver, Ed., *Microwave Antenna Theory and Design*, London, U.K.: Peregrinus, 1984.

[12] S. L. Johns and A. Prata Jr., "An improved raised-cosine feed model for reflector antenna applications," in *Proc. IEEE AP-S Int. Symp.*, Seattle, WA, June 1994, pp. 970–973.

Fernando J. S. Moreira (S'89–M'98) was born in Rio de Janeiro, Brazil, on July 18, 1967. He received the B.S. and M.S. degrees from Catholic University, Rio de Janeiro, in 1989 and 1992, respectively, and the Ph.D. degree from the University of Southern California, Los Angeles, in 1997, all in electrical engineering.

He is currently an Associate Professor of the Department of Electronics Engineering, Federal University of Minas Gerais, Brazil. His research interests are in the areas of electromagnetics, antennas, and propagation. He has authored or coauthored more than 20 journal and conference papers in these areas. He

Dr. Moreira is a member of Eta Kappa Nu and the Brazilian Microwave and Optoelectronics Society.

Aluizio Prata, Jr. (S'84–M'90) was born on March 18, 1954, in Uberaba, Brazil. He received the B.S.E. degree from the University of Brasilia, Brasilia, Brazil, in 1976, the M.S. degree from the Pontifical Catholic University of Rio de Janeiro, Rio de Janeiro, Brazil, in 1979, and the Ph.D. degree from the University of Southern California, Los Angeles, in 1990, all in electrical engineering. He received the M.S.E.E. degree from the California Institute of Technology, Pasadena, in 1984.

From 1979 to 1983 he was with the Telebras research and development center, Brazil, working on the design and construction of satellite earth station antennas. While with the California Institute of Technology, he designed and implemented one of the first operational neural computers. Currently, he is an Assistant Professor at the University of Southern California, working with applied electromagnetics. He has been a Consultant for several aerospace companies. He has authored or coauthored more than 50 articles, patents, and symposium papers.

Dr. Prata is a member of Sigma Xi and Eta Kappa Nu. He is a past Chair of the Los Angeles Chapter of the IEEE Antennas and Propagation Society.